Cooperative Navigation between a Ground Vehicle and an Unmanned Aerial Vehicle in GNSS-Challenged Environments

Victor O. Sivaneri, Jason N. Gross, *West Virginia University*

ABSTRACT

This paper considers cooperative navigation between a Unmanned Aerial Vehicle (UAV) in a GNSS-challenged environment with an Unmanned Ground Vehicle (UGV), and focuses on the design of the optimal motion of the UGV to best assist the UAV's navigation solution. Our approach reduces the uncertainty of a UAV's navigation solution through the use of radio ranging updates from a cooperative UGV. In this study, we develop and compare two novel methods for designing a UGV's trajectory such that the UAV's dilution of precision is reduced. To conduct this study, a simulation environment is used to characterize the performance of the cooperative navigation between a UAV and a UGV. The study is conducted to evaluate the positioning accuracy during common GNSS-challenged scenarios such as: a vehicle in an urban environment and flying against a building. Using an Ultra Wideband (UWB) radio, the UAV in a GNSS-challenged environment, an urban canyon, is able to determine it's position with the support of a UGV. The use of a UGV and moving it based on the reduction of dilution of precision, has shown to decrease the position error of the UAV.

1 INTRODUCTION

Collaborative navigation is a research area that has been increasingly active in recent years, especially in support of military operations and Intelligent Transportation Systems (ITS) (Strömbäck et al., 2010). This is due to the fact that these environments are oftentimes GNSS-challenged. In military situations, UAVs or UGVs, may go from situations where GNSS is readily available to completely denied (e.g., being jammed or traversing inside a cave). The major downside of GNSS is that it requires an open-sky (Kealy et al., 2015). In military operations, sub-meter level accuracy and high update rates (e.g., > 10 Hz) are needed, and this is not always possible with standalone GNSS (Zador et al., 2000). In the context of ITS, urban canyons often lead to extreme multipath and GNSS outages, which can cause positioning errors as large as a few hundred meters (Ko et al., 2015). These scenarios are a few of the better-known cases when cooperative navigation would be beneficial. Other cases include, UAVs for bridge inspection or structural health monitoring (Guo et al., 2011), UAVs for surveillance in urban environments (Alam et al., 2013), or UAVs transitioning from indoor-to-outdoor or vice versa (Serranoa et al., 2014).

To improve the positioning solution, multi-sensor integration has to be considered. As discussed in Titterton and Weston (2005), a number of techniques have been introduced to combat the issues in GNSS-challenged conditions, such as Inertial Navigation Systems (INS) and odometers; but it is well known that these sensors diverge rapidly over time and will not be able to handle long GNSS outages and multipath.

Collaborative positioning techniques, such as using local measurements between vehicles or nodes, have helped tackle this problem. Collaborative navigation uses many sensors to aid in navigating when GNSS is degraded or not available. These sensors include Inertial Measurement Units (IMU), inter-nodal raging, lasers, cameras, magnetometers, and various other aides. Many collaborative navigation techniques focus on the use of Vehicle Ad-Hoc Networks (VANETs), where multi-sensor fusion is used on individual nodes, and the collaboration between nodes is opportunistic in nature. Most of the collaborative navigation communication is with Dedicated Short Range Communications (DSRC) for vehicle-to-vehicle and vehicle-to-infrastructure communication (Kealy et al., 2015).

The typical approaches used in DSRC are Angle of Arrival (AoA) and Time of Arrival (ToA). The AoA positioning technique measures the angle between the reference nodes and the target nodes. ToA, used for Ultra WideBand (UWB) radios, rely on the travel time of the measurement from the reference node to the target nodes (Gezici et al., 2005). An advantage of using UWB signals is they have been shown to work in non-LOS application, can penetrate walls, and are not significantly impacted by multipath (Gao et al., 2014). Another benefit using the UWB radios, are their weight and cost.

Kassas and Humphreys (2013) used signal of opportunities, radio signals, to draw navigation and timing information. The authors found that adopting a information-based optimal motion planning performed better than having a pre-described path. The optimal motion planning evaluated different actions that the receiver could take, then move to a location that would maximize the information about the environment. The use of an cooperative navigation algorithm to navigate vehicles through a field with obstacles, has been seen in Ferrari et al. (2011). In this case, the UAV provides a low resolution map to the UGV, so it can plan it's movements based on the objects ahead. However, this requires the UGV to be in the field of view of the UAV which does not help in urban canyons, as the GNSS information would be the same for both vehicles.

Using peer-to-peer updates for positioning is not new, as there is plenty of research that has been conducted on stationary nodes (Bais and Morgan, 2012) (Kealy et al., 2015) and on moving nodes (Gao et al., 2014) (Parker and Valaee, 2007) (Kassas and Humphreys, 2013). For example, Bais and Morgan (2012) evaluated the best position for placing base stations, to have the area covered by 4 base stations at all times. Gao et al. (2014) investigated using UWBs on a vehicle-to-vehicle platform, where the vehicles exchanged their position with each other. Hardy et al. (2016) and Strader et al. (2016) focused on the design and evaluation of an estimation strategy for determining the relative pose of the aircraft, between UAVs in a GPS-denied environment. On the contrary, there has been less of an emphasis on the control or design for the location of the cooperative navigation nodes.

In this paper, the use of cooperative navigation is investigated between a UGV and a UAV, in which a DSRC consisting of a UWB radio, is used to provide range measurements between the two vehicles and the UGV is strategically moved in order to reduce the Position Dilution of Precision (PDOP) of the UAV. PDOP was chosen as our basis for designing the UGVs trajectory because it well-known that the PDOP is essential in determining the accuracy of a positioning system (Misra and Enge, 2006). In this setting, the following is taken advantage of: (1) the UGV has a non-degraded GNSS solution, (2) a single UGV acting as a ranging source is able yield a wide range of unit vectors with respect to the location of a UAV, and (3) a UGV is naturally positioned to improve a UAV's solution geometric as it emanates its ranging signal from a direction that a GNSS transmitter cannot. By leveraging these characteristics, this cooperative navigation algorithm yields increased accuracy of the positioning of the UAV faced with GNSS-challenged conditions.

The rest of this paper is organized as follows. Section 2 motivates our cooperative approach by assessing the effectiveness of a single ranging sources ability to reduce PDOP when given the freedom of the transmitter location. Section 3 describes the algorithm formulation of the cooperative navigation for both without the UGV and with the UGV. Next, Sections 4 and 5 presents the results of a series of simulations. Finally, Section 6 discusses the conclusion of the study and future planned experimental work.

2 CONCEPT OVERVIEW

Figure 1 shows the assumed set-up for the cooperative navigation in an urban canyon. The UAV is in a GNSS-challenged environment (e.g. under forest cover, urban canyon, bridge inspection). It is furthered assumed that the cooperative vehicle is not GNSS-challenged. A UGV is initially being assumed as the cooperative vehicle, but the technology being discussed herein is not restricted to use on a UGV. This only simplifies the ability to realize an experimental demonstration.

2.1 Review of PDOP

Dilution of Precision (DOP) provides a simple characterization of the user-satellite geometry. The better the geometry, the lower the DOP, the better the position estimate. Starting from the Linear Least Squares (LLS) GNSS-solution,

$$\Delta x = (G^T G)^{-1} G^T \Delta\rho \tag{1}$$

where G is the "Geometry Matrix". The pseudorange measurement model is given by the equation

$$\rho_C^k = r^k + c\delta t_u + \tilde{\varepsilon}_\rho^k \tag{2}$$

where r^k is the geometric range from satellite k to the user, c is the speed of light, δt_u is the receiver clock bias, and $\tilde{\varepsilon}_\rho^k$ is the measurement residuals, where it is assumed that the measurement residuals are zero-mean $E[\tilde{\varepsilon}_\rho]$, and the variance of the error is given by

$$E[\tilde{\varepsilon}_\rho \tilde{\varepsilon}_\rho^T] = P_\varepsilon = \sigma_{URE}^2 \mathbf{I} \tag{3}$$

where σ_{URE} is the standard deviation of the "User Range Error" and is provided by the GPS control segment. Using the LLS solution, the clock bias estimation, and the zero-mean assumption, the estimation covariance matrix can be formed

$$cov[\Delta x] = \sigma_{URE}^2 (\mathbf{G}^T \mathbf{G})^{-1} = \sigma_{URE}^2 \mathbf{H} \tag{4}$$

where G is the Geometry Matrix and ρ is the pseudorange measurement. The Geometry Matrix is constructed by creating a set of unit vectors, of the distance between the satellites and the UAV position. Within this study, the Geometry Matrix is augmented by the UWB measurement from the UGV, which effectively acts as another satellite observation.

where $\mathbf{H}^{DOP}$ is formed as shown in Eq. 5

$$\mathbf{H}^{DOP} = (\mathbf{G}^T \mathbf{G})^{-1} = \text{diag}\begin{bmatrix} H_{11}, & H_{22}, & H_{33}, & H_{44} \end{bmatrix} \tag{5}$$

The Root Mean Square (RMS) of the 3D position is known as the Position Dilution of Precision (PDOP),

$$PDOP = \sqrt{\mathbf{H}_{11}^{DOP} + \mathbf{H}_{22}^{DOP} + \mathbf{H}_{33}^{DOP}} \tag{6}$$

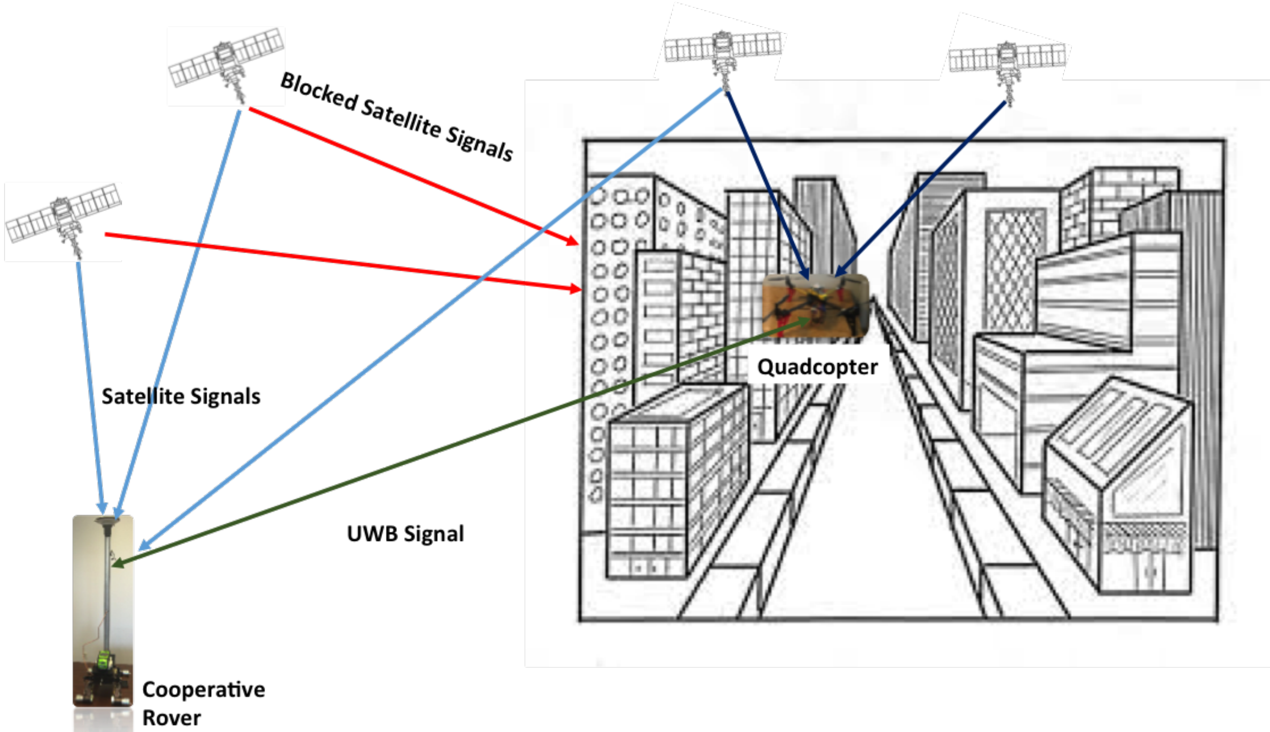

Figure 1. Concept Diagram for Cooperative Navigation with UWB Ranging between a UAV and UGV

2.2 Reducing PDOP with a Single Ranging Source

To motivate the potential of this approach, a simple Monte-Carlo simulation was conducted to determine the maximum amount of PDOP reduction that could be realized by the addition of a single ranging source, for different GNSS satellite geometries. That is, the location of the simulated user location and the GNSS time of week was randomized in order to realize a large number of constellation geometries for a given scenario. Next, to simulate a GNSS-challenged condition, high azimuth and elevation masks were applied to simulate a user's GNSS visibility being impacted. As a single example, Figure 2 shows the percentage of PDOP reduction that could occur, with the inclusion of a UWB ranging source located in the best position within a 25 m square grid surrounding the UAV's location, as a function of the GNSS-only PDOP.

In Figure 2, a 180 degree azimuthal mask and 50 degree elevation mask was used to simulate a UAV up against a tall building. From this analysis, it is apparent that the poorer the satellite geometry, the more beneficial the single ranging source can become. For example, the PDOP can reduced by 90 % when the initial PDOP is 10 (i.e. the PDOP can be reduced to as low as 1). However, the minimum potential PDOP reduction is also shown to motivate the fact that the cooperative ranging source must be strategically placed. That is, the additional ranging source could offer little or no benefit if poorly located.

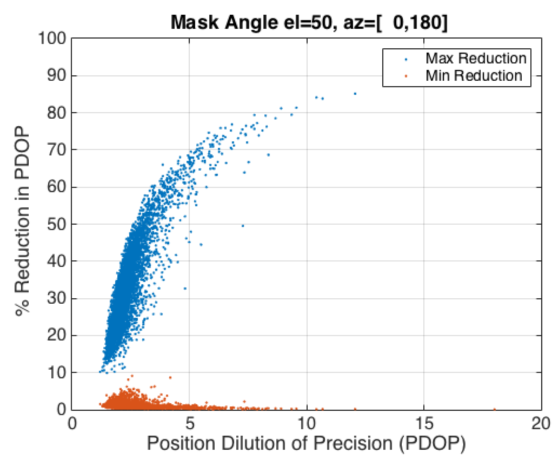

Figure 2. Monte Carlo simulation result that illustrates the potential improvement of including a single additional ranging source that is optimally placed.

3 ALGORITHM FORMULATION

This section gives an overview of the formulations used in this paper. First an overview of the GNSS/INS filter design is discussed, then how the UWB is implemented in the GNSS/INS filter, and finally the cooperative strategy, locally greedy and regionally optimal, used for the UGV and the UAV.

3.1 Core GNSS/INS Filter Design

The GNSS/INS integration filter adopted uses INS error-state formulation with closed-loop feedback, which corrects the integrated INS solution at each time step. The INS estimated navigation states are used to predict the GNSS-observable within the EKF. The estimated state vector is,

$$\mathbf{x} = \begin{bmatrix} \delta\Psi \\ \delta v \\ \delta r \\ b_a \\ b_g \\ \delta t_u \\ \dot{\delta t}_u \\ T_w \\ N_1 \\ \vdots \\ N_j \end{bmatrix} \tag{7}$$

where $\delta\Psi$ is the INS attitude error, δv is the INS velocity error, δr is the INS position error, b_a is the Inertial Measurement Unit (IMU) tri-axial accelerometer sensor biases, b_g is the (IMU) tri-axial gyroscope sensor biases, δt_u is the estimated receiver clock bias, $\dot{\delta t}_u$ is the estimated receiver clock drift, T_w is the estimated troposphere, and $N_{1..j}$ is the estimated phase bias for each satellite in view. For the attitude update, a 3^{rd} order fixed-step Runge-Kutta integration method was used for the integration of the quaternion, which represents the UAV's body attitude in the Earth Centered Inertial (ECI) frame (Jekeli, 2001). For this study, an error-state Kalman Filter is being used, where the formulation for the position, attitude, and velocity equations are from Groves (2013). For the complete details of the GNSS/INS formulation adopted, the reader is referred to (Gross et al., 2015) and (Watson et al., 2016).

3.2 GNSS/INS Augmentation with UWB Ranges

The GNSS observation matrix, $\mathbf{H}^{obs}$, is dependent on the number of satellites in view, and the number of states estimated, as shown above in the state vector Eq. 7, which is 18. It represents the sensitivity of the observed measurement models to the state being estimated. The first 6 columns of $\mathbf{H}^{obs}$ correspond to, the INS attitude and velocity errors and are zero as they do not appear in the GNSS pseudorange and carrier-phase observation models. The next 3 columns of $\mathbf{H}^{obs}$ are the partials of user's ECI position. Columns 10-15 of $\mathbf{H}^{obs}$ are the partials of the IMU sensors biases which are modeled with random-walk dynamics and therefore zero, and column 16 is the partial derivative of the GNSS receiver clock bias. In this study, no GNSS receiver clock drift is estimated, therefore clock drift partial is zero. The troposphere's zenith delay partials are comprised of the elevation dependent mapping function, and appear in column 18 of $\mathbf{H}^{obs}$. The rest of the columns are populated with an identity matrix over the block of rows that correspond to the carrier-phase observations. This identity matrix represents the partial derivative of the carrier-phase observational model with respect to the carrier-phase biases. This is the $\mathbf{H}^{obs}$ matrix when the UGV is not being used. The size of the $\mathbf{H}^{obs}$ matrix is shown in Eq. 8

$$\mathbf{H}^{obs} = [2 * S \quad , \quad N + S] \tag{8}$$

where S is the number of GNSS satellites in view and N is the number of non phase-bias states estimated. When the UGV is employed, $\mathbf{H}^{obs}$ only slightly differs. The UGV is considered as an additional GNSS satellite measurement, but this measurement only has partial for the position as it does not have a receiver clock bias, troposphere delay, or a carrier-phase bias.

$$\mathbf{H}^{obs} = \begin{bmatrix} 0_{1x6} & u_X & u_Y & u_Z & 0_{1x6} & 1 & 0 & M_{el} & 0_{nxn} \\ \vdots & \vdots & \vdots & \vdots & \vdots & \vdots & \vdots & \vdots & \\ 0_{1x6} & u_X & u_Y & u_Z & 0_{1x6} & 1 & 0 & M_{el} & I_{nxn} \\ \vdots & \vdots & \vdots & \vdots & \vdots & \vdots & \vdots & \vdots & \\ 0_{1x6} & uwb_X & uwb_Y & uwb_Z & 0_{1x6} & 0 & 0 & 0 & 0_{1xn} \end{bmatrix} \tag{9}$$

where n is the number of satellites in view. The UWB range, distance between the UAV and UGV, is implemented as an observation in the z_k vector and is shown in Eq. 10.

$$y_{uwb} = ||pos_{UAV} - pos_{UGV}||_2 \tag{10}$$

To include the UWB ranging source, the UWB range must be predicted for inclusion in the filter. Then the difference between the UWB predicted range and the UWB measured range was inserted at the end of the z_k vector.

$$z_k = \begin{bmatrix} \Delta\rho_1 \\ \vdots \\ \Delta\rho_N \\ \Delta\Phi_1 \\ \vdots \\ \Delta\Phi_N \\ \Delta UWB \end{bmatrix} \tag{11}$$

where $\Delta\rho$ is the Observed Minus Computed (OMC) pseudorange of the satellites in view, $\Delta\Phi$ is the OMC carrier phase of the satellites in view, and the ΔUWB is OMC UWB range, where the computed is the distance between the UAV and UGV.

A simple UWB error model was parameterized by empirically modeling the UWB ranging errors with two Time Domain P410 Ranging and Communication Radio Modules (RCM). These tests consisted of both line-of-sight (LoS) and non-line-of-sight (NLoS). The following Figures 3, 4, and 5 show one of the test set-ups, the corresponding error history, and the histogram, respectively.

The mean and standard deviation of the error were 6140 mm and 28 mm, respectively. In the filter, a normal distribution of 5 cm was added to the UWB measurement as a conservative bound of the empirically estimated distribution.

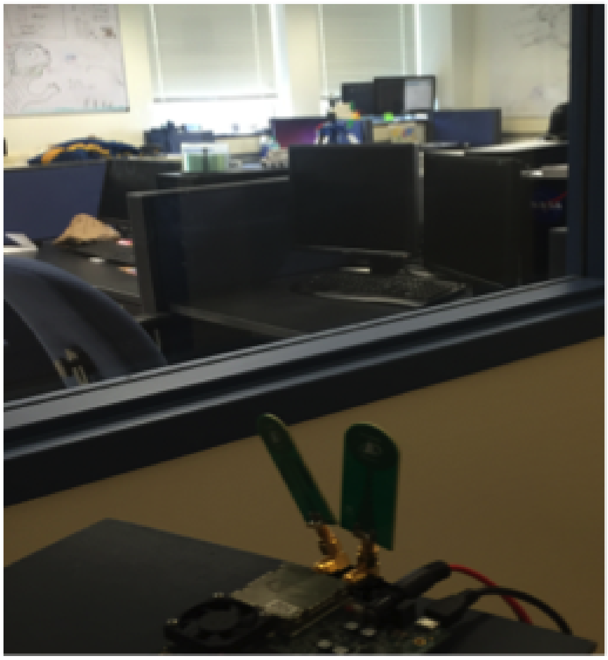

Figure 3. Set up for short range Non Line of Sight (NLoS) ranging testing.

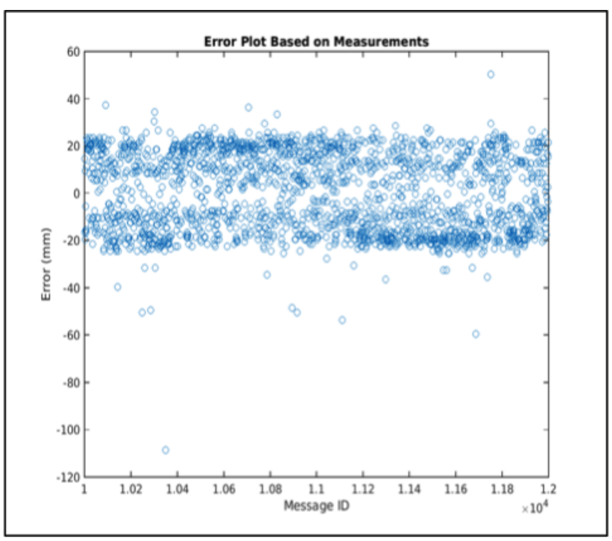

Figure 4. Time history of ranging errors for short range NLOS.

3.3 Cooperative Strategy

The two strategies that were evaluated included: (1) having the UGV choose the minimum PDOP, of the UAV, if it were to select from points immediately around the UGV, and (2) having the UGV calculate the minimum PDOP, of the UAV, it it were to be located anywhere within a 50 meter by 50 meter grid centered at the UAV, then moving in the regionally optimal direction. For both approaches, the maximum distance that the UGV is assumed to move over one GNSS measurement updated interval is 1 meter.

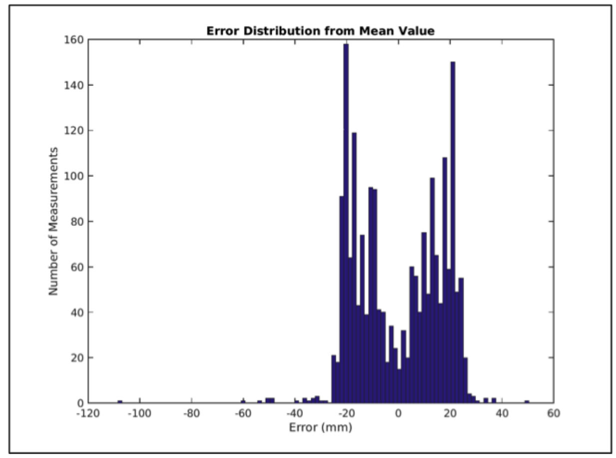

Figure 5. Distribution of ranging errors for short range NLOS.

3.3.1 Locally Greedy Strategy

In this approach, first the UAV captures the signals from all available GNSS satellites to calculate is position solution. After the UAV communicates the satellites it has in view, the UGV determines which location it should move, Eq. 12, in order to reduce the PDOP. This is accomplished by the UGV calculating what the UAV's PDOP would become when incorporating a UWB ranging update from each of the UGV's candidate locations. With the Locally Greedy approach, the list of candidate position includes of all positions immediately surrounding the UGV. The number of positions evaluated that encircle the UGV was set to 10.

To implement this approach, 10 candidate UGV heading angles, $\Psi^{\ell=1:10} = \left[0, \quad \ldots \quad, 2\pi\right]$, were selected and candidate positions were calculated using Eq. 12.

$$r_{k+1}^{UGV,ENU^{\ell}} = \begin{bmatrix} r_k^{UGV,E} + d * cos(\Psi^{\ell}) \\ r_k^{UGV,N} + d * sin(\Psi^{\ell}) \\ 0 \end{bmatrix} \tag{12}$$

where $r_{k+1}^{UGV,ENU^{\ell}}$ is the UGV's candidate location for heading angle Ψ^{ℓ}, $r_k^{UGV,E}$ is the UGV's current East position, $r_k^{UGV,N}$ is the UGV's current North position, d is the move distance of the UGV, Ψ^{ℓ} is the candidate heading location around the rover that is being evaluated. With each candidate UGV location, the UAV's GNSS-only Geometry Matrix, G, is augmented using unit vector to the candidate UGV position and current best estimate of the UAV's position

$$u_{uwb} = \frac{r_k^{UAV} - r_{k+1}^{UGV,ENU^{\ell}}}{||r_k^{UAV} - r_{k+1}^{UGV,ENU^{\ell}}||_2} \tag{13}$$

where the u_{uwb} is the unit vector distance between the UAV and the candidate UGV position. With the set of UAV Geometry matrices augmented with each UGV candidate location, the PDOP for each candidate 1 to ℓ is evaluated, and the minimum PDOP is selected as indicated in Eq. 14.

$$minPDOP = argmin(PDOP_1 \quad \ldots \quad PDOP_N) \tag{14}$$

Once the minimum potential PDOP of the UAV is identified, the UGV is moved to the location that corresponds to the minimum UAV PDOP. Additional UGV path planning logic was also included to ensure that it does not get too close to the UAV. This is to ensure that the UGV doesn't also enter the GNSS-challenged environment. For the time being, this is implemented as a simple perimeter of radius 70 meters was set around the UAV's best known location and established a no-UGV-zone. As such, if the UGV's next desired trajectory position falls inside the perimeter, the following steps are taken. First, the slope of the distance between the UAV and UGV is found using Eq. 15.

$$m = \frac{\Delta r_N}{\Delta r_E} \tag{15}$$

where m is the slope, Δr_N is the North component of the distance between the UAV and UGV, and Δr_E is the East component of the distance between the UAV and UGV. Next, the intersection of the perimeter and the UGV, is determined, based on the slope and the equation for a circle as shown in Eq. 16 and 17 .

$$r_{k+1}^{UGV,E} = sign(r_k^{UGV,E})\sqrt{\frac{r_{perim}^2}{(m^2+1)}} \tag{16}$$

$$r_{k+1}^{UGV,N} = m r_k^{UGV,N} \tag{17}$$

where $r_{k+1}^{UGV,E}$ is the UGV's next East position, r_{perim} is the radius of the perimeter, and $r_{k+1}^{UGV,N}$ is the UGV's next North position. In Eq. 16, the *sign* operator is to ensure rover is located in the proper quadrant of the circle. For future development of this approach, *a prior* map information will be included in this part of the trajectory design for selection of the perimeter.

3.3.2 Regionally Optimal Strategy

For the regionally optimal cooperative UGV path planning strategy, a 50 meter by 50 meter grid is setup with the UAV at the center. Then, UWB-augmented-PDOP from including a ranging observation that is emanating from every point on the grid is computed. As an example of this approach, Figure 6 shows the percentage reduction possible for the 50 meter by 50 meter grid at one time step, for one simulation scenario. The yellow represents a region in which a 60 % percentage reduction is achievable. After evaluating this grid, the minimum overall PDOP is determined as seen in Eq. 18.

$$minPDOP_{grid} = argmin(PDOP_{1grid} \quad \ldots \quad PDOP_{Ngrid}) \tag{18}$$

Once the east and north location of where the PDOP is minimum is found, the UGV is driven in that direction. This is

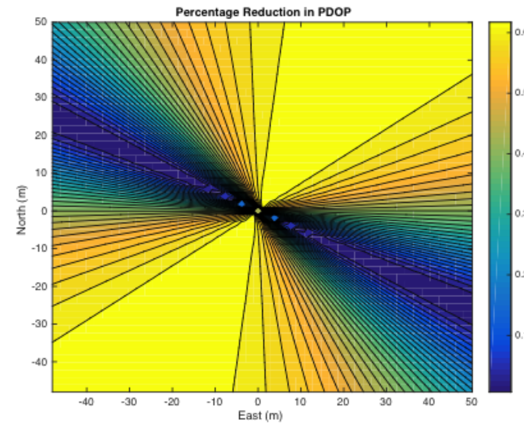

Figure 6. Regional optimal strategy using a grid to calculate minimum augmented-PDOP

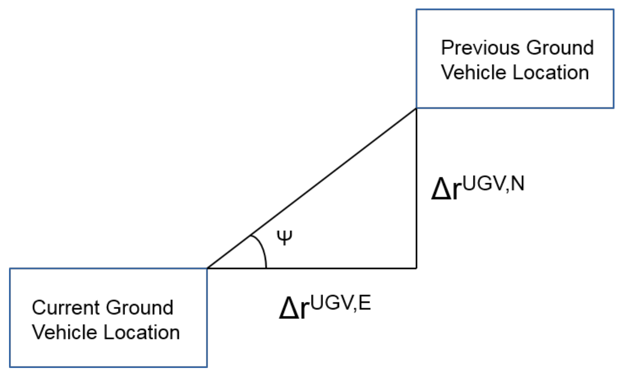

Figure 7. Diagram of heading calculation between two UGV locations.

accomplished by first determining the distance between the current UGV position and the location where the PDOP of the UAV is minimum over the grid as shown in Eq. 19 and 20.

$$\Delta r^{UGV,E} = r_k^{UGV,E} - E_{PDOPmin}^{Grid} \tag{19}$$

$$\Delta r^{UGV,N} = r_k^{UGV,N} - N_{PDOPmin}^{Grid} \tag{20}$$

where $E, N_{PDOPmin}^{Grid}$ is the location where the PDOP would be minimized for the rover location within the grid. From here, the heading angle, Ψ, is found to determine which direction the UGV should move, as seen in Figure 7. The heading was calculated by Eq. 21.

$$\Psi = atan2(\Delta r^{UGV,N}, \Delta r^{UGV,E}) \tag{21}$$

Since there is a constraint that the UGV can only move a maximum of 1 meter per time step, the next UGV location is determined based on the move distance and the heading, Eq. 22 and 23.

$$r_{k+1}^{UGV,E} = r_k^{UGV,E} + d * cos(\Psi) \tag{22}$$

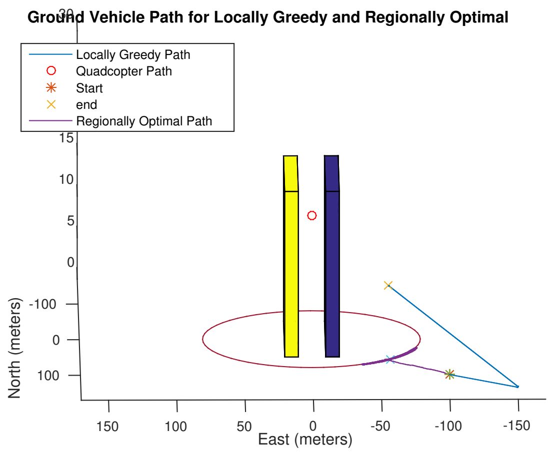

Figure 8. Example of locally greedy and regionally optimal path in a GNSS-challenged environment

$$r_{k+1}^{UGV,N} = r_k^{UGV,N} + d * sin(\Psi) \tag{23}$$

where d is the maximum move distance of the UGV and Ψ is the heading angles. As stated above, there is a check in place to make sure the UGV does not come too close to the UAV. If it does, the same procedure described in Section 3.3.1.

4 SIMULATION ENVIRONMENT

The raw GNSS and IMU data used in the simulation was generated using a commercially available SatNav-3.04 and Inertial–Navigation Toolboxes **(GPSoft 2003)**, which is a GNSS constellation simulation toolbox. Inputs that were defined for the generation of GPS and IMU data, were the origin in Latitude, Longitude, and Height, the time of the week, and the length of the flight. These inputs were selected at random, giving each case different satellite geometry and atmospheric effects. For more information on the generation of data, please refer to (Watson et al., 2016) for a more detailed description.

The particular error source important to this study was GNSS multipath errors. As such, for this work the multipath error was increased to simulate the GNSS- challenged environment of an urban-canyon. Multipath was modeled as a first order Guass-Markov error source and with a σ =8 meters and a time constant, τ of 2 minutes. Furthermore, to simulate a GNSS-challenged environment, an elevation and azimuth mask, i.e. buildings in an urban canyon, was incorporated as seen in Figure 8. The masks were held constant throughout the simulated flight, and for all data sets. This simulation also included an orbit error model to represent the errors in the GNSS broadcast ephemeris. The satellite ephemeris errors were modeled by differencing the broadcast products provided by the International GNSS Service (IGS) and the Center for Orbit Determination (CODE). A multi-sinusoidal model was fitted

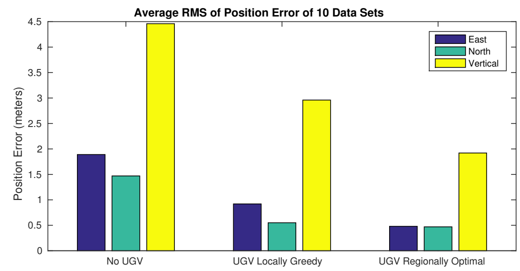

Figure 9. Average RMS of 10 data sets

to the error, and based on the time of day. More information can be found in Watson et al. (2016). The UAV and UGV were assumed to start at arbitrary positions. Within this study Monte-Carlo design was implemented and 10 data sets were generated.

5 RESULTS

The generated data sets were run through the GNSS/INS filter with and without augmentation from the UGV in order to characterize the performance of including a cooperative UGV. Next, both cooperative strategies were attempted such that any differences between the two different approaches would become apparent. In Figure 9, the first graph shows the GPS position error when having a UGV employing the locally greedy cooperative strategy, the second is when the UGV is using the regionally optimal strategy, and the last one is without having a UGV. Table 1 shows the average RMS values for the East, North, and Vertical position error. It can be seen that having a UGV employing the locally greedy strategy is better than having no UGV, and having a UGV employing the regionally optimal strategy is the best scenario.

Table 1. Average RMS of 10 data sets

	E. (m)	**N. (m)**	**V. (m)**
No Ground Vehicle	1.89	1.47	4.46
Locally Greedy	0.92	0.55	2.96
Regionally Optimal	0.48	0.47	1.92

In Figure 10, the first graph shows the multi-constellation, GNSS, position error when having a UGV employing the locally greedy cooperative strategy, the second is when the UGV is using the regionally optimal strategy, and the last one is without having a UGV. Table 2 shows the average GNSS RMS values for the East, North, and Vertical position error. As with the GPS case, having no UGV is the worst scenario, but for the GNSS case, the locally greedy scenario was the best case. In all scenarios for GNSS, the RMS values were less than the GPS-only case.

The next figures detail a specific example of one simulation trial in which the UGV's path and the reduction in PDOP are shown. Figure 11 shows the path that the UGV

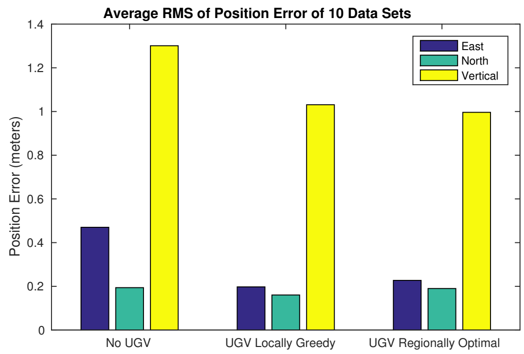

Figure 10. Average RMS of 10 data sets

Table 2. Average RMS of 10 data sets

	E. (m)	**N. (m)**	**V. (m)**
No Ground Vehicle	0.47	0.19	1.30
Locally Greedy	0.19	0.16	1.03
Regionally Optimal	0.22	0.19	0.99

takes when employing both the locally greedy path and the regionally optimal path. The $*$ is where the UGV starts, and the x is where it ends. The blue line indicates the locally greedy path, and the green line indicates the regionally optimal path. The circle is the perimeter that the UGV is not allowed to cross. The locally greedy UGV, moves toward the UAV in the East direction, but has no change in the North direction. Whereas the regional optimal strategy moves toward the UAV, then moves along the constraint boundary. This is expected, as we can see from Figure 6, the largest reduction of PDOP matches the path of the UGV with regionally optimal strategy employed.

Figure 12 shows the PDOP over the entire flight for having no UGV,the UGV employing the locally greedy al-

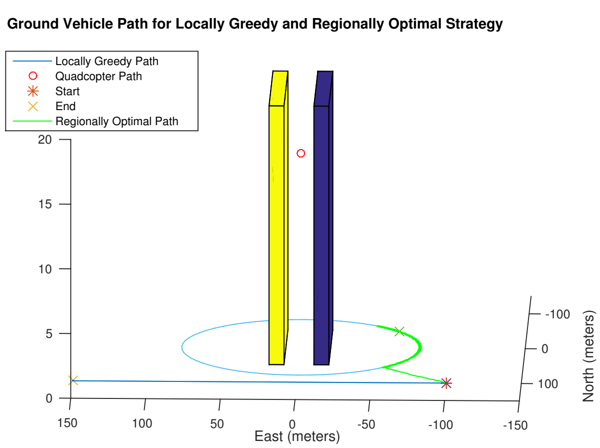

Figure 11. UGV's path, Regionally Optimal and Locally Greedy, in a GNSS-challenged environment

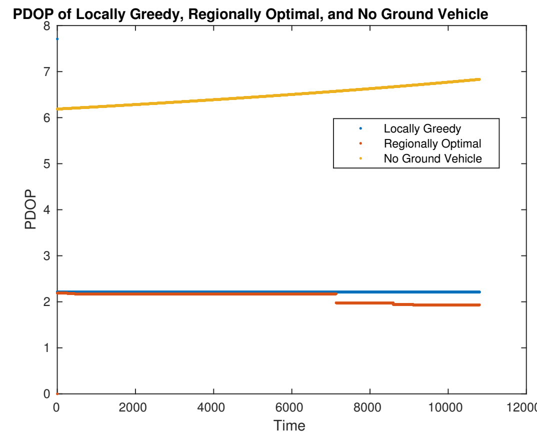

Figure 12. PDOP without UGV, UGV locally greedy, and UGV Regionally Optimal

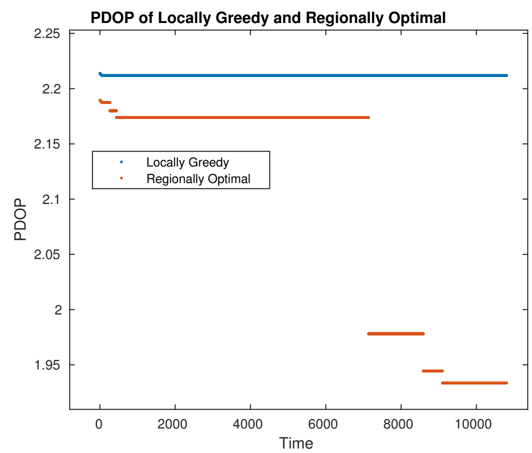

Figure 13. PDOP when using a UGV Locally Greedy, and UGV Regionally Optimal

gorithm, and the UGV employing the regionally optimal approach. The PDOP when having the UGV is much less than when there is no UGV. It can be seen how much an effect having a UGV's ranging source can have on the PDOP. Figure 13 shows the comparison of PDOP while using a UGV with a regionally optimal strategy and the locally greedy strategy. The PDOP for the regionally optimal algorithm is reduced further than that of the locally greedy path planning approach.

6 CONCLUSIONS

A cooperative navigation strategy has been employed to improve the positioning of a UAV in a GNSS-challenged environment. This paper described the filter design, cooperative techniques, and a simulation evaluation. As expected, having a UGV ranging source has been shown to help in the positioning of the UAV whenever it was cooperatively located. This work has shown that employing different cooperative strategies for trajectory planning of the UGV has an effect on the vehicle positioning. The regionally optimal strategy performed better than the locally greedy strategy. Future work will consider implementing a differential-type filter between the two vehicles, and an experimental flight-test evaluation.

ACKNOWLEDGEMENTS

This work was supported in part NGA Academic Research Program (NARP) Grant # HM0476-15-1-0004. Approved for public release under case number 16-523.

REFERENCES

P. Strömbäck, J. Rantakokko, S.-L. Wirkander, M. Alexandersson, K. Fors, I. Skog, and P. Händel, "Foot-mounted inertial navigation and cooperative sensor fusion for indoor positioning," in *ION International Technical Meeting (ITM)*, 2010.

A. Kealy, G. Retscher, C. Toth, A. Hasnur-Rabiain, V. Gikas, D. Grejner-Brzezinska, C. Danezis, and T. Moore, "Collaborative navigation as a solution for pnt applications in gnss challenged environments–report on field trials of a joint fig/iag working group," *Journal of Applied Geodesy*, vol. 9, no. 4, pp. 244–263, 2015.

P. Zador, S. Krawchuk, and R. Vocas, "Final report–automotive collision avoidance (acas) program," Technical Report DOT HS 809 080, NHTSA, US DOT, Tech. Rep., 2000.

H. Ko, B. Kim, and S.-H. Kong, "Gnss multipath-resistant cooperative navigation in urban vehicular networks," *Vehicular Technology, IEEE Transactions on*, vol. 64, no. 12, pp. 5450–5463, 2015.

Y. Guo, F. Wan, L. Wu, and H. Jiang, "Research of structural health monitoring based on mode analysis for uav wings," in *Prognostics and System Health Management Conference (PHM-Shenzhen), 2011*. IEEE, 2011, pp. 1–4.

N. Alam, A. Kealy, and A. G. Dempster, "Cooperative inertial navigation for gnss-challenged vehicular environments," *Intelligent Transportation Systems, IEEE Transactions on*, vol. 14, no. 3, pp. 1370–1379, 2013.

D. Serranoa, M. U. de Haag, E. Dill, S. Vilardaga, and P. Duan, "Seamless indoor-outdoor navigation for unmanned multi-sensor aerial platforms," *The International Archives of Photogrammetry, Remote Sensing and Spatial Information Sciences*, vol. 40, no. 3, p. 115, 2014.

S. Gezici, Z. Tian, G. B. Giannakis, H. Kobayashi, A. F. Molisch, H. V. Poor, and Z. Sahinoglu, "Localization via ultra-wideband radios: a look at positioning aspects for future sensor networks," *Signal Processing Magazine, IEEE*, vol. 22, no. 4, pp. 70–84, 2005.

Y. Gao, X. Meng, C. M. Hancock, S. Stephenson, and Q. Zhang, "Uwb/gnss-based cooperative positioning method for v2x applications," in *Proceedings of the 27th International Technical Meeting of the ION Satellite Division, ION GNSS+ 2014*. ION, 2014, pp. 3212–3221.

Z. Kassas and T. Humphreys, "Motion planning for optimal information gathering in opportunistic navigation systems," in *Proceedings of AIAA Guidance, Navigation, and Control Conference*, 2013, pp. 4551–4565.

S. Ferrari, M. Anderson, R. Fierro, and W. Lu, "Cooperative navigation for heterogeneous autonomous vehicles via approximate dynamic programming," in *Decision and Control and European Control Conference (CDC-ECC), 2011 50th IEEE Conference on*. IEEE, 2011, pp. 121–127.

A. Bais and Y. Morgan, "Evaluation of base station placement scenarios for mobile node localization," in *Mobile, Ubiquitous, and Intelligent Computing (MUSIC), 2012 Third FTRA International Conference on*. IEEE, 2012, pp. 201–206.

R. Parker and S. Valaee, "Cooperative vehicle position estimation," in *ICC*, 2007, pp. 5837–5842.

J. Hardy, J. Strader, J. N. Gross, Y. Gu, M. Keck, J. Douglas, and C. N. Taylor, "Unmanned aerial vehicle relative navigation in gps denied environments," in *2016 IEEE/ION Position, Location and Navigation Symposium (PLANS)*. IEEE, 2016, pp. 344–352.

J. Strader, Y. Gu, J. N. Gross, M. De Petrillo, and J. Hardy, "Cooperative relative localization for moving uavs with single link range measurements," in *2016 IEEE/ION Position, Location and Navigation Symposium (PLANS)*. IEEE, 2016, pp. 336–343.

P. Misra and P. Enge, *Global Positioning System: Signals, Measurements and Performance Second Edition*. Lincoln, MA: Ganga-Jamuna Press, 2006.

C. Jekeli, *Inertial navigation systems with geodetic applications*. Walter de Gruyter, 2001.

P. D. Groves, *Principles of GNSS, inertial, and multisensor integrated navigation systems*. Artech House, 2013.

J. N. Gross, R. M. Watson, V. Sivaneri, Y. Bar-Sever, W. Bertiger, and B. Haines, "Integration of inertial navigation into real-time gipsy-x (rtgx)," in *Institute of Navigation GNSS+*. Tampa, FL: ION, 2015.

R. M. Watson, V. Sivaneri, and J. N. Gross, "Performance characterization of tightly-coupled gnss precise point positioning inertial navigation within a simulation environment," in *2016 AIAA Guidance Navigation and Control Conference. AIAA*, 2016.